

# 1 Shoreline instability under low-angle wave incidence

D. Idier

2 BRGM, 3 Avenue C. Guillemin, BP 6009, 45060 Orléans Cedex 2, France

A. Falqués

3 UPC, C/ Jordi Girona 1-3, Modul B4/B5, despatx 103 - E-08034, Barcelona,

4 Catalonia, Spain

B.G. Ruessink

5 Utrecht University, Institute for Marine and Atmospheric Research Utrecht,

6 Faculty of Geosciences, Department of Physical Geography, P.O. box 80115,

7 3508 TC Utrecht, The Netherlands

R. Garnier

8 Instituto de Hidráulica Ambiental IH Cantabria, Universidad de Cantabria,

9 ETSI Caminos Canales y Puertos, Avda. los Castros s/n, 39005 Santander,

10 Cantabria, Spain

---

D. Idier, BRGM, 3 Avenue C. Guillemin, BP 6009, 45060 Orléans Cedex 2, France.

(d.idier@brgm.fr)

A. Falqués, UPC, C/ Jordi Girona 1-3, Modul B4/B5, despatx 103 - E-08034, Barcelona,

Catalonia, Spain. (falques@fa.upc.edu)

11 **Abstract.**

12 The growth of megacusps as shoreline instabilities is investigated by ex-  
13 amining the coupling between wave transformation in the shoaling zone, long-  
14 shore transport in the surf zone, cross-shore transport, and morphological  
15 evolution. This coupling is known to drive a potential positive feedback in  
16 case of very oblique wave incidence, leading to an unstable shoreline and the  
17 consequent formation of shoreline sandwaves. Here, using a linear stability  
18 model based on the one-line concept, we demonstrate that such instabilities  
19 can also develop in case of low-angle or shore-normal incidence, under cer-  
20 tain conditions (small enough wave height and/or large enough beach slope).  
21 The wavelength and growth time scales are much smaller than those of high-  
22 angle wave instabilities and are nearly in the range of those of surf zone rhyth-  
23 mic bars,  $O(10^2 - 10^3 \text{ m})$  and  $O(1 - 10 \text{ days})$ , respectively. The feedback  
24 mechanism is based on: (1) wave refraction by a shoal (defined as a cross-  
25 shore extension of the shoreline perturbation) leading to wave convergence  
26 shoreward of it, (2) longshore sediment flux convergence between the shoal  
27 and the shoreline, resulting in megacusp formation, and (3) cross-shore sed-

---

B.G. Ruessink, Utrecht University, Institute for Marine and Atmospheric Research Utrecht,  
Faculty of Geosciences, Department of Physical Geography, P.O. box 80115, 3508 TC Utrecht,  
The Netherlands. (b.g.ruessink@uu.nl)

R. Garnier, IH Cantabria, Universidad de Cantabria, Avda. los Castros s/n, 39005 Santander,  
Cantabria, Spain. (garnierr@unican.es)

28 iment flux from the surf to the shoaling zone, feeding the shoal. Even though  
29 the present model is based on a crude representation of nearshore dynam-  
30 ics, a comparison of model results with existing 2DH model output and lab-  
31 oratory experiments suggests that the instability mechanism is plausible. Ad-  
32 ditional work is required to fully assess whether and under which conditions  
33 this mechanism exists in nature.

## 1. Introduction

Rhythmic shorelines featuring planview undulations with a relatively regular spacing or wavelength are quite common on sandy coasts. In the present study, we focus on undulations that are linked to submerged bars or shoals and are generally known as shoreline sandwaves [Komar, 1998; Bruun, 1954]. These sandwaves can be classified according to their length scale as short and long sandwaves (see, e.g., Stewart and Davidson-Arnott [1988]).

The spacing of short sandwaves ranges from several tens to several hundreds of meters and their seaward perturbations are known as megacusps. Observations show that these megacusps can develop shoreward of crescentic bar systems during the typical “Rhythmic Bar and Beach” morphological beach state or can develop from the shore attachment of transverse bars that characterise the “Transverse Bar and Beach” state [Wright and Short, 1984]. These transverse bars can appear where the horns of a previous crescentic bar approach the shoreline [Wright and Short, 1984; Sonu, 1973; Ranasinghe et al., 2004; Lafon et al., 2004; Castelle et al., 2007]. On the other hand, transverse bars can also develop freely, independently of any offshore rhythmic system (e.g. the “transverse finger bars” [Sonu, 1968, 1973; Ribas and Kroon, 2007]). The formation of rhythmic surf zone bars and associated megacusps is believed to be due primarily to an instability of the coupling between the evolving bathymetry and the distribution of wave breaking (bed-surf coupling) [Falqués et al., 2000]. The developing shoals and channels cause changes in wave breaking, which in turn cause gradients in radiation stresses and thereby horizontal circulation with rip currents. If the sediment fluxes carried by this circulation converge

55 over the shoals and diverge over the channels, a positive feedback arises and the coupled  
56 system self-organizes to produce certain patterns, both morphological and hydrodynamic  
57 (see, e.g., *Reniers et al.* [2004]; *Garnier et al.* [2008]). In the case of oblique wave inci-  
58 dence, a meandering of the longshore current is also essential to the instability process  
59 [*Garnier et al.*, 2006]. Two important characteristics of all available models of the self-  
60 organized formation of rhythmic surf zone bars are that they (1) are essentially based  
61 on sediment transport driven by the longshore current and rip currents only, i.e. ignore  
62 cross-shore transport induced by undertow and wave non-linearity and (2) do not consider  
63 morphological changes beyond the offshore reach of the rip-current circulation.

64 Rhythmic shorelines can also develop as a result of an instability not related to bed-  
65 surf coupling. *Ashton et al.* [2001] and *Ashton and Murray* [2006a, b] have shown that  
66 sandy shorelines are unstable for wave angles (angle between wave fronts and the local  
67 shoreline orientation) larger than about  $42^\circ$  in deep water, leading to the formation of  
68 shoreline sandwaves, cusped features and spits. *Falqués and Calvete* [2005] have found  
69 that the initial characteristic wavelength of the emerging sandwaves is in the range of 3 to  
70 15 km, i.e., much larger than that of surf zone rhythmic bars. This instability caused by  
71 high-angle waves will henceforth be referred to as HAWI (High-Angle Wave Instability).  
72 The physical mechanism can be explained as follows. For oblique wave incidence, there  
73 are essentially two counteracting effects. On one hand, the angle relative to the local  
74 shoreline is larger on the lee of a cusped feature than on the updrift side. This tends to  
75 cause larger alongshore sediment flux at the lee and thereby divergence of sediment flux  
76 along the bump, which therefore tends to erode. On the other hand, since the refractive  
77 wave ray turning is stronger at the lee than at the updrift flank, there is more wave energy

78 spreading due to crest stretching at the lee causing smaller waves and smaller alongshore  
79 sediment flux. This produces convergence of sediment flux at the bump, which therefore  
80 tends to grow. For high angle waves the latter effect dominates and, if the bathymetric  
81 perturbation associated with the shoreline feature extends far enough offshore, it leads to  
82 the development of the cusped feature. In contrast to the bed-surf instability for rhythmic  
83 surf zone bars, this instability mechanism depends essentially on the coupling between the  
84 surf and shoaling zones. Indeed, the gradients in alongshore sediment flux that induce  
85 bathymetric changes in the surf zone occur because of wave field perturbations induced by  
86 bathymetric features in the shoaling zone. Thus, in order to achieve a positive feedback,  
87 the shoals (or the bed depressions) in the surf zone must extend into the shoaling zone.  
88 This is achieved by the cross-shore sediment fluxes induced, for instance, by wave non-  
89 linearity, gravity and undertow, which force the cross-shore shoreface profile to reach an  
90 equilibrium profile. HAWI may provide an explanation for the self-organized formation  
91 of some long shoreline sand waves which are reported in the literature [*Verhagen, 1989*;  
92 *Inman et al., 1992*; *Thevenot and Kraus, 1995*; *Ruessink and Jeuken, 2002*; *Davidson-*  
93 *Arnott and van Heyningen, 2003*].

94 On the other hand, some observations for low incidence angles show that longshore  
95 currents can converge on megacusps because of wave refraction [*Komar, 1998*]. Such cur-  
96 rent convergence may lead to longshore sediment flux convergence and hence to megacusp  
97 growth. If the submerged part of the megacusp grows and extends far enough into the  
98 shoaling zone (due to the cross-shore transport leading to an equilibrium profile), wave  
99 refraction would be enhanced and a positive feedback would arise. This might provide a  
100 mechanism for shoreline instability formation under low-angle wave incidence that bears

101 some similitude with HAWI in the sense that the coupling between the surf and shoaling  
102 zones is essential, in contrast to the bed-surf instability. We will refer to this potential  
103 mechanism as Low-Angle Wave Instability (LAWI). The aim of the present contribution  
104 is to investigate this new morphodynamic instability mechanism and discuss whether the  
105 resulting shoreline instability may be found in nature.

106 The lay-out of this paper is as follows. First (Section 2), we introduce the 1D-morfo  
107 model [*Falqués and Calvete, 2005*] that we used to investigate LAWI. Numerical experi-  
108 ments of idealized cases are presented and analyzed in Section 3. We find that shoreline  
109 sandwaves can indeed develop because of LAWI, with a length scale comparable to those  
110 of megacusps and rhythmic surf zone bars. In Section 4, we analyze the physics of the  
111 instability mechanism. We conclude our paper with a discussion and a summary of the  
112 main results.

## 2. The shoreline stability model: 1D-morfo

113 Owing to the similitude with HAWI [*Ashton et al., 2001; Falqués and Calvete, 2005*], the  
114 LAWI mechanism is assumed to be un-related to surf zone processes like rip or longshore  
115 meandering currents. Thus, the engineering simplification of one-line modeling [*Dean*  
116 *and Dalrymple, 2002*] is used, where the shoreline dynamics are based on alongshore  
117 gradients in the total alongshore transport rate,  $Q$  (i.e., the total volume of sand carried  
118 by the wave-driven longshore current that crosses a cross-section of the surf zone area  
119 for unit of time ( $m^3/s$ )). Using such a simple model, which neglects numerous aspects  
120 of surf zone dynamics, including rip current circulation, longshore current meandering,  
121 and thus the bed-surf coupling phenomena, allows to investigate properly whether the  
122 LAWI mechanism is supported by the governing equations. Furthermore, the consistency

123 of the sediment transport patterns from the one-line modelling has been confirmed by  
124 using a 2DH model (delft3D) [List and Ashton, 2007], at least in case of HAWI. These  
125 reasons, in addition to the fact that HAWI has been studied and reproduced with a linear  
126 stability model called 1D-morfo based on the one-line concept, lead us to use the same  
127 model to investigate LAWI and its differences with HAWI. A very brief description of the  
128 1D-morfo model is given here. The reader is referred to *Falqués and Calvete* [2005] for  
129 further details.

130 The model describes the dynamics of small amplitude perturbations of an otherwise rec-  
131 tilinear coastline. Following the one-line concept, the dynamics are governed by gradients  
132 in the total alongshore wave-driven transport rate  $Q$ :

$$\bar{D} \frac{\partial x_s}{\partial t} = - \frac{\partial Q}{\partial y} \quad (1)$$

133 A Cartesian coordinate system is used, with  $x$  increasing seaward in the unperturbed  
134 cross-shore direction and  $y$  running alongshore (Figure 1). The position of the shoreline  
135 is given by  $x = x_s(y, t)$ , where  $t$  is time and  $\bar{D}$  is the active water depth (as defined by  
136 *Falqués and Calvete* [2005]), which is of the order of the depth of closure. This active  
137 water depth is directly related to the one-line model concept, for more details, see *Falqués*  
138 *and Calvete* [2005]. The transport rate  $Q$  is computed according to the longshore sediment  
139 transport equation of *Ozasa and Brampton* [1980]. In this formulation,  $Q$  is the sum of  
140 two terms: the first one ( $Q_1$ ) is driven by waves approaching the shore at an angle and  
141 is equivalent to the CERC formula [USACE, 1984], and the second one ( $Q_2$ ) takes into  
142 account the influence of wave set-up induced currents related to the alongshore gradient  
143 in the wave height.

**Figure 1**



144 The equation of the sediment transport rate  $Q$  can be written as follows:

$$Q = Q_1 + Q_2 \quad Q = \mu H_b^{5/2} \left( \sin(2(\theta_b - \phi)) - r \frac{2}{\beta} \cos(\theta_b - \phi) \frac{\partial H_b}{\partial y} \right) \quad (2)$$

145 where  $H_b$  is the (rms) wave height at breaking (index  $b$ ),  $\theta_b$  is the angle between wave  
146 fronts and the unperturbed coastline at breaking, and  $\phi = \tan^{-1}(\partial x_s / \partial y)$  is the local  
147 orientation of the perturbed shoreline.  $\beta$  is the beach slope at the instantaneous shoreline  
148 (i.e. the waterline). The constant  $\mu$  is proportional to the empirical parameter  $K_1$  of  
149 the original CERC formula and is  $\sim 0.1 - 0.2 \text{ m}^{1/2}\text{s}^{-1}$ . For the reference case of this  
150 paper, a value,  $\mu = 0.15 \text{ m}^{1/2}\text{s}^{-1}$ , was chosen, which corresponds to  $K_1 = 0.525$ . The  
151 nondimensional parameter  $r$  is equal to  $K_2/K_1$ , where  $K_2$  is the empirical parameter of  
152 *Ozasa and Brampton* [1980]. According to *Horikawa* [1988],  $r$  ranges between 0.5 and 1.5,  
153 whereas *Ozasa and Brampton* [1980] suggest a value of 1.62. The value  $r = 1$  is used for  
154 the present reference case, which is equivalent to  $K_2 = K_1$  and has been used in several  
155 earlier studies on shoreline instabilities [*Bender and Dean*, 2004; *List et al.*, 2008; *van den*  
156 *Berg et al.*, 2011]. However, the term  $Q_2$  is not always taken into account, and its validity  
157 and application range are uncertain. In section 3.2, we will study the sensitivity of our  
158 results to the value of  $r$ .

159 Some discussion exists about the capacity of the CERC formula ( $Q_1$ ) to predict correctly  
160 gradients in alongshore sediment transport in the presence of bathymetric perturbations  
161 [*List et al.*, 2006, 2008; *van den Berg et al.*, 2011]. The results of *List and Ashton* [2007]  
162 suggest that the CERC formula predicts qualitatively correct transport gradients for large  
163 scale shoreline undulations (alongshore lengths of 1-8 km). The term  $Q_2$  was introduced to  
164 describe the sediment transport resulting from alongshore variations in the breaker wave  
165 height induced by diffraction near coastal structures. These breaker-height variations in-

166 duce alongshore gradients in set-up, which drive longshore currents and hence sediment  
167 transport. In our work, alongshore variability in breaker heights is related to wave re-  
168 fraction rather than to wave diffraction, but the subsequent mechanism for alongshore  
169 sediment transport remains the same.

170 To compute the sediment transport rate according to eq. 2,  $H_b(y, t)$  and  $\theta_b(y, t)$  are  
171 needed. The procedure to determine them is as follows. It is assumed that the wave  
172 height and wave angle are alongshore uniform in deep water. Then, wave transformation,  
173 including refraction and shoaling, is performed from deep water up to the breaking point  
174 so that  $H_b(y, t)$  and  $\theta_b(y, t)$  are determined and  $Q$  can be computed. To do the wave  
175 transformation, a perturbed nearshore bathymetry coupled to the shoreline changes is  
176 assumed:

$$D(x, y, t) = D_0(x) - \beta f(x) x_s(y, t) \quad (3)$$

177 where  $D(x, y, t)$  and  $D_0(x)$  are the perturbed and unperturbed water depth, respectively,  
178 and  $f(x)$  is a shape function. Figure 2a shows some examples of possible perturbation  
179 profiles: constant bed perturbation in the surf zone and decreasing exponentially in the  
180 offshore direction (P1), bed perturbation decreasing exponentially in the offshore direction  
181 from the coast (P2), and bed perturbation similar to a shoal (P3 and P4).

**Figure 2**

182 The offshore extension of the bathymetric perturbation is controlled by its “charac-  
183 teristic” length,  $xl$ , which is a free parameter in the model. It was shown by *Falqués*  
184 *and Calvete* [2005] that the coupling between the surf and shoaling zones is crucial for  
185 HAWI. This is accomplished only if  $xl$  is at least a couple of times larger than the surf  
186 zone width. The parameter  $xl$  can be seen as a way to parameterise cross-shore sediment  
187 transport, especially between the surf and shoaling zones. This makes HAWI essentially

188 different from the surf zone morphodynamic instabilities that lead to rhythmic bars and  
189 rip channels. The changes in the shoreline cause changes in the bathymetry (both in the  
190 surf and shoaling zones), which in turn cause changes in the wave field. The changes in  
191 the wave field affect the sediment transport that drives shoreline evolution. Therefore,  
192 the shoreline, the bathymetry and the wave field are fully coupled.

193 Following the linear stability concept, the perturbation of the shoreline is assumed to  
194 be

$$x_s(y, t) = ae^{\sigma t + iKy} + c.c. \quad (4)$$

195 where  $a$  is a small amplitude. For each given (real) wavenumber,  $K$ , this expression is  
196 inserted into the governing equation (eq. 1), and into the perturbed bathymetry equation  
197 (eq. 3). By computing the perturbed wave field and inserting  $H_b$  and  $\theta_b$  in eq. 1, the  
198 complex growth rate,  $\sigma(K) = \sigma_r + i\sigma_i$ , is determined. All of the equations are linearized  
199 with respect to the amplitude,  $a$ . Then, for those  $K$  such that  $\sigma_r(K) > 0$  a sandwave with  
200 wavelength  $\lambda = 2\pi/K$  tends to emerge from a positive feedback between the morphology  
201 and the wave field. The pattern that has the maximum growth rate is called the Linearly  
202 Most Amplified mode (LMA mode).

### 3. Numerical experiments on idealised cases

203 To investigate the possible mechanism causing shoreline instabilities under low wave  
204 incidence angles, numerical experiments on idealised cases are performed. First, numerical  
205 experiments and results are given. Then, a sensitivity study is done to assess better the  
206 results.

### 3.1. Instabilities versus beach slope and wave incidence angle

#### 3.1.1. Configuration

A Dean profile (Figure 2b) is chosen as the equilibrium profile, using various beach slopes (Figures 2b and c). The adopted profile is given by:

$$D_0(x) = b \left( (x + x_0)^{2/3} - x_0^{2/3} \right) \quad (5)$$

which has been modified from the original Dean profile to avoid an infinite slope at the shoreline. The constants  $b$  and  $x_0$  are determined from the prescribed slope  $\beta$  at the coastline and the prescribed distance  $x_c$  from the coastline to the location of the closure depth  $D_c$  (see *Falqués and Calvete* [2005] for details). The forcing conditions are waves with  $H_{rms} = 1.5$  m and  $Tp = 8$  s at a water depth of 25 m. The wave direction ranges from  $0^\circ$  to  $85^\circ$  in increments of  $5^\circ$ . A closure depth  $\bar{D} = 20$  m is chosen. To perform the linear stability analysis, the shape function for the bathymetric perturbations is assumed to be constant in the surf zone and to decrease exponentially seaward. Its cross-shore extent is given by the characteristic distance  $xl$  corresponding to the closure depth of 20 m, i.e.  $xl = 1410$  m for the present case (P1-perturbation in Figure 2a).

#### 3.1.2. Results

Figure 3a shows the growth rate of the LMA mode versus the wave angle and the beach slope. The wave angle is given for a water depth of 25 m. The beach slope is defined as the beach slope at the shoreline. For small beach slopes ( $< 0.04$ ) the coast behaves as expected: it is unstable only if the wave incidence angle is large enough. In this case, the shoreline instabilities clearly correspond to HAWI. For instance, for a beach slope of 0.02,

**Figure 3**

226 a wave incidence of  $70^\circ$  leads to the largest growth rate ( $3.13 \times 10^{-9} \text{ s}^{-1}$ ), corresponding  
227 to a wavelength of 7000 m (Figure 3b).

228 However, for larger beach slopes, instabilities occur for all wave directions, and espe-  
229 cially for low wave incidence angles. These instabilities correspond to what will be called  
230 LAWI in the present paper. Furthermore, among all the wave incidence angles, the most  
231 amplified mode is for shore-normal wave incidence. For a beach slope of 0.1, an angle of  
232  $0^\circ$  leads to the largest growth rate ( $1.82 \times 10^{-6} \text{ s}^{-1}$ ), corresponding to a wavelength of  
233 571 m (Figure 3b).

### 3.2. Sensitivity analysis

234 The sensitivity analysis is performed using a planar beach, as the aim is to focus on the  
235 mechanisms. However, simulations with other (e.g. barred) profiles also lead to LAWI  
236 (not shown).

#### 3.2.1. Wave height and beach slope

238 Keeping the same reference configuration as above and focusing on shore-normal wave  
239 incidence, we investigate the sensitivity of the instability to the wave height for a range  
240 of beach slopes. For normally incident waves, instabilities develop only for a beach slope  
241 that exceeds 0.04 (Figure 4). In this case, there is an optimum in the wave height for  
242 which the growth rate is largest. This wave height increases with the beach slope. For  
243 instance, for a beach slope of 0.1 and 0.18), the optimal wave height  $H_{rms}$  is 1.75 m and  
244 2.5 m, respectively. A wave height increase also leads to an increase in the LMA mode  
245 wavelength, which is due to the corresponding increase in surf zone width.

**Figure 4**

#### 3.2.2. Bathymetric perturbation length

247 The influence of the parameter  $xl$  was previously investigated by *Falqués and Calvete*  
248 [2005], who showed that  $xl$  must exceed a threshold to initiate HAWI (the perturbation  
249 must extend across both the surf and shoaling zones). Similar behaviour is found here  
250 by exploring the range between  $xl = 10$  and  $xl = 10^4$  m. Figure 5 shows that there is a  
251 threshold,  $xl > 100$  m, above which shoreline instabilities may occur. This value appears  
252 physically reasonable since the width of the surf zone in the reference case is about 73  
253 m. For  $125 \leq xl \leq 250$  m, the shoreline instability wavelength decreases significantly  
254 (from 1040 to 530 m) with increasing perturbation length, whereas for  $xl \geq 250$  m, the  
255 wavelength increases only slightly until reaching a nearly constant value of 574 m. The  
256 growth rate increases with increasing  $xl$  for values below 500 m but decreases for  $xl$   
257 exceeding 500 m, reaching a nearly constant value for large perturbation length scales.  
258 The main conclusion is that instabilities occur only if the perturbation extends far enough  
259 into the shoaling zone. When the perturbation length is about the width of the surf zone,  
260 it influences the wavelength and growth rate of the LMA mode strongly, whereas for larger  
261 perturbation length values, this influence is negligible.

**Figure 5**

### 262 **3.2.3. Initial perturbation shape**

263 To evaluate the influence of the bathymetric perturbation shape function on the results  
264 we have presented so far, several shapes were investigated using the same wave-boundary  
265 conditions and a perturbation length  $xl$  of 2000 m. The shape functions we consider are  
266 (Figure 2a):

- 267 • Perturbation P1: bed perturbation constant in the surf zone and decreasing expo-  
268 nentially in the offshore direction

269 • Perturbation P2: bed perturbation decreasing exponentially from the coast in the  
270 offshore direction

271 • Perturbation P3: P2 perturbation with a shoal located only in the shoaling zone,  
272 from 400 to 800 m, with a maximum height at  $x_1 = 600$  m.

273 • Perturbation P4: P2 perturbation with a shoal located in both the surf and shoaling  
274 zones, from 0 to 1400 m, with a maximum height at  $x_1 = 600$  m.

275 The reference configuration is still the same ( $H_{rms}=1.5$  m,  $T = 8$  s,  $\theta = 0^\circ$ ). The four  
276 shape functions result in LMA mode wavelengths of 571, 571, 608 and 608 m, respectively,  
277 and growth rates of 1.7, 1.5, 1.7,  $1.7 \times 10^{-6}$  s<sup>-1</sup>, respectively. Thus, the results are  
278 slightly sensitive (mean wavelength of 598 m and a standard deviation of 18 m) to the  
279 bed perturbation type, but all perturbation types cause LAWI with similar growth rates.

#### 280 3.2.4. Sediment transport equation

281 To investigate the sensitivity of the results to the sediment transport equation, compu-  
282 tations were carried out with  $r = 0$ , which reduces eq. 2 to the CERC equation. This  
283 sensitivity study is done in beach slope - wave angle space. The LMA characteristics are  
284 quite similar with  $r = 1$  (Figure 3) and  $r = 0$  (Figure 6), except for the case of normal  
285 wave incidence. In this case ( $r = 0$ ), for small beach slopes, all of the perturbations are  
286 damped, as for  $r = 1$ . For larger beach slopes, the growth rate increases with decreasing  
287 perturbation wavelength without reaching a local maximum (Figure 7). Thus there is no  
288 LMA mode for shore-normal wave incidence (X symbol on Figure 6). This specific case for  
289 shore-normal wave incidence will be discussed in section 4. To summarize, the previous  
290 results are not highly sensitive to the second term of the sediment transport equation,  
291 except for the case of shore-normal wave incidence.

**Figure 6**

**Figure 7**

## 4. The physical mechanism

292 Here we investigate the physics behind the model prediction of shoreline instabilities  
 293 caused by low wave incidence angles. The physical processes are analysed based on the  
 294 study of the growth rate components, and the hydrodynamic and sediment transport  
 295 patterns, before identifying the main mechanisms.

### 4.1. Growth rate analysis

296 In the perturbed situation where the shoreline position is given by eq. 4, the wave  
 297 height and wave angle at breaking are given by:

$$\begin{aligned}
 H_b(y, t) &= H_b^0 + (\hat{H}'_{br} + i\hat{H}'_{bi})e^{\sigma t + iKy} + c.c. \\
 \theta_b(y, t) &= \theta_b^0 + (\hat{\theta}'_{br} + i\hat{\theta}'_{bi})e^{\sigma t + iKy} + c.c.
 \end{aligned}
 \tag{6}$$

298 where  $H_b^0, \theta_b^0$  are the wave height and angle for the unperturbed situation. Then, according  
 299 to *Falqués and Calvete* [2005], the growth rate (the real part of the complex growth rate)  
 300 is:

$$\sigma_r = \underbrace{2\frac{\mu}{D}H_b^0K^2\cos(2\theta_b^0)}_{e_0} \left( \underbrace{-1}_{e_1} + \underbrace{\frac{\hat{\theta}'_{bi}}{aK}}_{e_2} + \underbrace{\frac{5\hat{H}'_{bi}}{4aKH_b^0}\tan(2\theta_b^0)}_{e_3} - r \underbrace{\frac{\hat{H}'_{br}\cos(\theta_b^0)}{a\beta\cos(2\theta_b^0)}}_{e_4} \right)
 \tag{7}$$

301 A clue to the physical mechanism is provided by a careful analysis of the meaning and  
 302 behaviour of each term:

303 •  $e_0$ : common to all terms. It does not contribute to the stability/instability since it  
 304 is positive. This is because we can assume that  $\theta_b^0 < 45^\circ$  due to wave refraction. It is the  
 305 magnitude of the growth rate.

306 •  $e_1$ : always negative. It represents the contribution due to the changes in shoreline  
 307 orientation when there is no perturbation in the wave field. This is the only term arising



308 in case of the classical analytical one-line modeling (Pelnard-Considère equation) [Dean  
309 and Dalrymple, 2002]. It is a damping term describing the shoreline diffusivity in that  
310 approach.

311 •  $e_2$ : its sign depends on  $\hat{\theta}'_{bi}$ . Numerical computations [Falqués and Calvete, 2005]  
312 demonstrates that it is always positive. This results from the fact that refracted wave  
313 rays tend to rotate in the same direction as the shoreline. Thus  $e_2$  is a growing term.

314 •  $e_3$ : its sign depends on  $\hat{H}'_{bi}$ . Numerical computations [Falqués and Calvete, 2005]  
315 show that  $\hat{H}'_{bi} > 0$  for long sandwaves and  $< 0$  for short sandwaves. This term is related  
316 to energy spreading due to wave crest stretching as waves refract. Thus  $e_3$  is a growing or  
317 damping term, depending on the sandwave wavelength,  $2\pi/K$ . Moreover, its magnitude  
318 increases with an increasing incident wave angle. These two properties explain that  $e_3$  is  
319 an essential growing term for HAWI formation Falqués and Calvete [2005], whereas, for  
320 LAWI, its magnitude is smaller and it is, most of the time, negative.

321 •  $e_4$ : this term stems from the alongshore gradients in  $H_b$  in the sediment transport  
322 equation (eq. 2). Its sign is the opposite to that of  $\hat{H}'_{br}$ , which is numerically found to be  
323 always positive. This is related to the fact that the maximum in wave energy is always  
324 located close to the sandwave crest (wave focusing). Thus  $e_4$  is a damping term.

325 The corresponding growth rate contributions,  $\sigma_1 = e_0e_1$ ,  $\sigma_2 = e_0e_2$ , ... are plotted in  
326 Figure 8. It can be seen that  $\sigma_2$  is always positive leading to the development of shoreline  
327 sandwaves, whereas  $\sigma_1$  and  $\sigma_4$  are always negative, leading to the damping of the sand-  
328 waves. The term  $\sigma_3$  can be either positive, for small beach slope (eg smaller than 0.05  
329 to 0.08), or negative, for larger beach slopes. Even if the behaviour of this term is not  
330 monotonous,  $\sigma_3$  generally increases with the wave angle. It is remarkable that  $\sigma_2$  becomes

**Figure 8**

331 very large for large beach slopes and for small wave angles. For normal wave incidence  
332 ( $\theta_b^0 = 0$ ),  $\sigma_3 = 0$  and  $\sigma_2$  is the only contribution leading to the instability. We therefore  
333 conclude that wave refraction is responsible for LAWI in the case of very steep beach  
334 slopes.

335 Based on the growth rate results, it is also possible to analyse the relative influence  
336 of the wave incidence induced  $Q_1$  and wave set-up induced  $Q_2$  sediment transport. The  
337 analysis of the growth rate versus the perturbation wavelength for  $r = 0$  or  $r = 1$  and  
338 several wave incidence angles  $\theta$  (Figure 9) shows that the relative influence of  $Q_2$  decreases  
339 with increasing the wave incidence angle. In other words, wave height gradients (wave set-  
340 up induced sediment fluxes) largely influence (damp) the shoreline instability for low wave  
341 angle incidence (LAWI), whereas their impact is almost negligible for large wave incidence  
342 angles (HAWI). The main driving term of the LAWI is due to the wave incidence induced  
343 sediment transport flux  $Q_1$ . This means that the use of the CERC equation alone, taking  
344 into account wave refraction in the shoaling zone, can cause LAWI. The  $Q_2$  term influences  
345 this instability by changing the growth rate and the favored wavelength. This influence  
346 increases with decreasing wave incidence until the case of perfectly shore-normal waves,  
347 for which there is a preferred wavelength (LMA mode) only if the  $Q_2$  term is taken into  
348 account (Figure 6).

**Figure 9**

## 4.2. Model results analysis: Hydrodynamic and sediment transport

349 To understand better how wave refraction causes shoreline instabilities, hydrodynamic  
350 and sediment transport model results are analysed next. Here, we focus on the case  
351 of shore-normal wave incidence, considering the LMA mode obtained for a beach slope  
352 equal to 0.1 (case a). The model results are compared with the same wave incidence, but

353 a smaller beach slope (0.02) for which the shoreline is stable (case b). The perturbation  
354 wavelength (571 m) is the same for both cases, corresponding to the LMA mode of case  
355 (a). Although the linear stability analysis is strictly valid only in the limit  $a \rightarrow 0$  we  
356 choose a shoreline sandwave amplitude  $a = 10$  m (for visualization and comparison of  
357 the different sources of sediment transport). In addition, to make the analysis simpler,  
358 we assume shore-normal waves and  $r = 0$ . Figures 10a and b show planviews of the  
359 wave angle, as well as a longshore cross-section of several quantities along the breaking  
360 line. First, it can be noted that the breaking line is much farther offshore in case (b)  
361 because of the shallower bathymetry. This is directly linked with the bathymetry. These  
362 planviews illustrate the wave focussing on the cusp, which implies increasing wave height  
363 and converging waves at the cusps.

364 Looking at the alongshore cross-section (Figure 10c), the wave angle amplitude is much  
365 larger for case (a) than for case (b), about  $14^\circ$  versus  $3.2^\circ$ , indicating a stronger refraction  
366 up to the breaking line in case (a). The corresponding amplitude of the oscillation in  
367 the shoreline angle is about  $6.3^\circ$ , and is thus within the range of those two values. This  
368 means that the angle of the wave fronts with respect to the local shoreline reverses when  
369 passing from case (a) to (b), implying a reversal in the direction of sediment transport.  
370 This can be traced back to equation 6. The wave angle amplitude is much larger for case  
371 (a). Coming back to equation 6, in the case of shore-normal waves and  $r = 0$ , there are  
372 only two terms left:  $e_1$ , which is the contribution due to shoreline change only, and  $e_2$ ,  
373 which represents the wave refraction-induced sediment flux. The analytical computation  
374 for the present case leads to:  $e_1 = -1$  for both cases, whereas  $e_2 = 2.23$  for case (a) and  
375  $e_2 = 0.507$  (case b), consistent with the different amplitudes of alongshore wave angle

Figures 10

376 oscillation. This clearly shows that the growth rate is positive for case (a) and negative  
377 for case (b). The alongshore cross-section of the resulting sediment flux  $Q$  (Figure 10c)  
378 illustrates the opposite behaviour for the two cases. Our sign convention is that positive  
379  $Q$  represents sediment transport directed in the direction of the increasing  $y$  coordinate  
380 (i.e. to the right on the cross-sections). A positive (negative) longshore gradient indicates  
381 a convergence (divergence), assumed to cause shoreline accretion (erosion). Thus Figure  
382 10c shows that  $Q$  for case (a) has a spatial phase-lag compared to the shoreline such that  
383 the shoreline perturbation should be amplified, whereas  $Q$  for case (b) has an opposite  
384 phase-lag, leading to the damping of the perturbation. This spatial phase-lag change  
385 results from the continuous amplitude changes of the terms  $e_1$  and  $e_2$ : the phase-lag  
386 between shoreline and longshore sediment fluxes is either  $90^\circ$  or  $-90^\circ$ , implying that  
387 there is no migration and either amplification or damping of the shoreline perturbation.  
388 Thus, for shore-normal waves and neglecting the damping term related with wave set-  
389 up induced sediment flux (second term in eq. 2), the instability of the shoreline results  
390 from an alongshore oscillation in the angle of wave refraction, which is stronger than the  
391 oscillation in the angle of shoreline orientation.

### 4.3. Mechanism

392 From the above, we can draw the following conclusion: the main growing term is re-  
393 lated to the wave refraction toward the cusp, leading to wave incidence induced sediment  
394 transport converging at the cusp. This term strongly increases with beach slope. The  
395 damping is due to three components: (1) longshore sediment transport due to the shore-  
396 line orientation only (and not refraction, term  $e_1$ ), (2) wave energy spreading (term  $e_3$ ),

397 and (3) wave height gradients (set-up) (term  $e_4$ ), the second component having a smaller  
398 damping effect than the two others.

399 Now we can figure out how LAWI works (Figure 11). Let us consider shore-normal  
400 wave incidence. In this case, the wave energy spreading has no influence on the instability  
401 ( $e_3 = 0$ ). If a cusped feature with an associated shoal develops on a coastline, wave  
402 refraction bends wave rays towards the tip of the feature. Depending on the orientation  
403 of the refracted wave fronts with respect to the local shoreline along the cusped feature,  
404 the alongshore sediment flux can be directed towards the tip, reinforcing it and leading to  
405 a positive feedback between flow and morphology. Whether the transport is directed to  
406 the tip, depends on the bathymetry and wave conditions. For a given offshore extent,  $xl$ ,  
407 of the associated shoal and a given wave height, the surf zone will become narrower if the  
408 beach slope increases. Then, the shoal will extend a longer distance beyond the surf zone,  
409 and the waves will be refracted strongly when they reach the breaking point, increasing  
410 the wave incidence related sediment flux ( $e_2$ ) convergence whereas the divergence term  
411 ( $e_1$ ) is constant. As shown by the model results (Figure 10), the contribution of the  
412 refracted wave angle ( $e_2$ ) can exceed the contribution of the shoreline orientation to the  
413 sediment flux ( $e_1$ ), such that  $Q_1$  (resulting from  $e_1$  and  $e_2$ ) converges near the cusp. This  
414 leads to the development of the cusp. If the beach slope is mild, the surf zone will be  
415 wider, and wave refraction over the shoal before breaking will be less intense, leading to  
416 smaller wave incidence angle induced sediment fluxes, which are dominated instead by the  
417 diverging sediment flux induced by shoreline orientation changes. In this case, as shown  
418 in the model results (Figure 10c), the sediment flux is directed away from the tip of the  
419 cusp.

**Figure 11**

## 5. Discussion

### 5.1. Linear stability analysis validity

420 The 1D-morfo model has been applied to investigate HAWI and to study the sandwaves  
421 generation along the Dutch coast [*Falqués, 2006*], El Puntal beach - Spain [*Medellín et al.,*  
422 2008, 2009]. The results indicated similarities with the wavelengths observed in nature.  
423 This supports the use of this linear stability model to investigate the mechanisms of shore-  
424 line sandwave formation. In the present paper, it is clear that LAWI is a robust output  
425 of the 1D-morfo model, and the physical mechanism causing instabilities is wave refrac-  
426 tion induced by an offshore shoal associated with a cusped feature. This wave refraction  
427 leads to two counter-acting phenomena: sediment transport induced by converging waves  
428 counteracted by diverging wave height gradients. The present paper investigates the lin-  
429 ear generation only. The pros and cons of linear stability analysis have been discussed  
430 extensively in [*Blondeaux, 2001; Dodd et al., 2003; Falqués et al., 2008; Tiessen et al.,*  
431 2010]. In any case, the fundamental assumption of infinitesimal amplitude growth makes  
432 comparisons to field data questionable. Nonlinear model studies for other rhythmic fea-  
433 tures, such as crescentic sandbars and sand ridges [*Calvete, 1999; Damgaard et al., 2002*],  
434 have sometimes shown the finite-amplitude dynamics to be dominated by the LMA mode  
435 ; in other cases, modes other than the LMA became dominant. We leave the nonlinear  
436 modeling of LAWI, including the study on cessation of the growth, to future work.

### 5.2. Analogy with megacusps: growth rates and circulation patterns

437 Although the model results are given for a planar beach, LAWI is also found in the  
438 presence of a shore-parallel bar (not shown). Thus, for intermediate morphological beach  
439 state where crescentic bars and associated megacusp systems usually develop, the model

440 predicts LAWI. To survive in the finite amplitude domain, the LAWI must grow at a  
441 rate comparable to that of co-existing instabilities. Our sensitivity studies indicate LAWI  
442 growth rates to range from  $10^{-6}\text{s}^{-1}$  (for a beach slope of 0.05) to  $10^{-5}\text{s}^{-1}$  (for a beach  
443 slope of 0.2). The typical generation time scale thus ranges from 1.5 to 11.5 days. These  
444 time scales were obtained for shore-normal waves having a moderate wave height of 1.5  
445 m and wave period of 8 s. A typical time scale for the LMA mode of crescentic bars is  
446 several days [Damgaard et al., 2002; Garnier et al., 2010]. Thus, for specific beach slope  
447 and wave conditions, the LMA shoreline instabilities have comparable initial growth rates  
448 as those of crescentic bar patterns.

449 Computations for the idealized cases gives LAWI wavelengths of the same order of  
450 magnitude as the observed spacing of crescentic bars and associated megacusps. The  
451 distinction between these two kinds of instabilities is therefore difficult and the validation  
452 of the presence of LAWI in a Rhythmic Bar and Beach morphological environment is not  
453 straightforward. More generally, a proper validation of the present results would need  
454 dataset of shoreline evolution, together with bathymetric, wave and current data, starting  
455 from an initial longshore uniform beach. To our knowledge, such data do not exist.

456 Although we cannot validate the model results with wavelengths observed in the field,  
457 it is possible to discuss whether the type of nearshore circulation linked to LAWI, that is,  
458 a longshore sediment flux pointing toward the cusped feature at both sides, is realistic or  
459 not in nature and in the framework of 2DH modeling. According to Komar [1998], both  
460 types of longshore current patterns, either converging or diverging at a megacusp, are  
461 observed in nature. Another example showing that this type of circulation is realistic is  
462 the case of a submerged breakwater. Both observations and numerical modelling indicate

463 that if the breakwater is beyond the breaker line, the waves drive longshore currents that  
464 converge at the lee of the breakwater to build a salient [Ranasinghe *et al.*, 2006]. This  
465 converging type of circulation at a megacusp was also observed by *Haller et al.* [2002] in  
466 laboratory experiments on barred beaches with rip channels. One of their six experimental  
467 configurations may be quite close to a LAWI configuration. This configuration had the  
468 largest average water depth at the bar crest and the smallest rip velocity at the rip neck,  
469 such that, in addition to the rip current circulation, they found a secondary circulation  
470 system near the shoreline, likely forced by the breaking of the larger waves that propagated  
471 through the channel. As these waves are breaking close to the shoreline, they drove  
472 longshore currents away from the rip channels into the shallowest area. This experiment  
473 shows that breaking close to the shoreline counteracts the rip-induced circulation, leading  
474 to current convergence in the shallowest area.

475 The studies of *Calvete et al.* [2005] and *Orzech et al.* [2011] give other elements to  
476 investigate the plausibility of the LAWI mechanism, in rip channels configurations. For  
477 the case of a barred-beach, *Calvete et al.* [2005] developed a 2DH linear stability model,  
478 having a fixed shoreline, that describes the formation of rip channels from an initially  
479 straight shore-parallel bar. For shore-normal waves, the circulation linked to rip channel  
480 formation is offshore through the channels and onshore over the shoals or horns of the  
481 developing crescentic bar as is clearly observed in nature (e.g. [MacMahan *et al.*, 2006]).  
482 However, they also noticed small secondary circulation cells near the shoreline flowing in  
483 the opposite direction, leading to presence of megacusp formed in front of the horns of  
484 the crescentic bar; therefore, the shoreline undulations were out of phase (spatial phase-  
485 lag of  $180^\circ$ ) with the crescentic bars, meaning that the amplitude of the wave-refracted



486 terms should dominate the amplitude of the wave set-up terms (Eq. 2). The formation of  
487 those megacusps was not part of the instability leading to the crescentic bar development  
488 but was forced by the hydrodynamics associated with it. More importantly, the small  
489 secondary circulation cells were essentially related to wave refraction: if wave refraction  
490 from the model was eliminated, they did not develop. Thus, wave refraction by offshore  
491 shoals (those of the crescentic bar in this case) can induce a circulation that may move  
492 sediment toward a developing cusped feature. A recent study, based on both observation  
493 (video images) and non-linear morphodynamic modeling [*Orzech et al.*, 2011] also showed  
494 the occurrence of two types of megacusp (shoreward of the shoal or shoreward of the  
495 rip), and the associated converging sediment fluxes toward the megacusps. This tends to  
496 support our mechanism analysis of LAWI formation.

497 The similarity between LAWI and megacusps in both wavelength and growth time  
498 is certainly intriguing given the fact that 1D-morfo is mainly based on the gradients  
499 in longshore sediment transport and wave set-up induced sediment transport (damping  
500 term), but neglects many surf zone processes like rip current circulation, which is known  
501 to be essential to crescentic bar dynamics [*Calvete et al.*, 2005; *Garnier et al.*, 2008].  
502 However, the analysis above tends to show that there could be configurations, where the  
503 processes taken into account in 1D-morfo are dominant in the system, at the initial stage.  
504 This could explain why similarities are observed with the various numerical experiments  
505 done with more sophisticated models. Furthermore, we should keep in mind the fact that  
506 the LAWI mechanism is not related to any longshore bar, and thus that short shoreline  
507 sandwaves such as megacusps could develop without a bar, whereas it was thought that,  
508 for barred beaches, short shoreline sandwaves develop due to surf zone sand bar variability.

## 6. Conclusions

509 A one-line linear stability model, which was initially created to describe the formation of  
510 shoreline sandwaves under high-angle wave incidence, has revealed shoreline instabilities  
511 for low to shore-normal wave incidence (LAWI). The most amplified mode has wavelengths  
512 of  $\sim 500$  m and characteristic growth time scales of a few days, which are smaller than  
513 those of the high angle wave instabilities. Sensitivity analyses focusing on wave height,  
514 wave incidence angle, beach slope, beach profile, model free parameters and the sediment  
515 transport equation show that, for low to shore-normal wave incidence, instabilities develop  
516 for sufficiently large beach slopes (e.g. 0.06) and for sufficiently small wave heights (smaller  
517 than 2 m for a beach slope of 0.06).

518 The main process causing the instabilities for low to shore-normal wave incidence is wave  
519 refraction on a shoal in the shoaling zone, which focuses wave fronts onshore of it, leading  
520 to wave incidence induced sediment transport converging at the cusp. This effect strongly  
521 increases with beach slope. The damping is due to three longshore transport components:  
522 (1) that caused by shoreline orientation only (and not refraction), (2) that caused by  
523 wave energy spreading (minor effect for low-angle wave incidence), (3) that caused by  
524 wave height gradients (set-up). Whether LAWI develops or not depends on the balance  
525 between these growing and damping terms. If this shoreline sand accumulation can feed  
526 the initial shoal through cross-shore sediment transport, a positive feedback arises.

527 **Acknowledgments.** The authors thank the reviewers (including A. Ashton) for their  
528 comments and suggestions, D. Calvete for fruitful discussions, J. Thiébot for his comments  
529 on this paper. M. Yates-Michelin is also acknowledged for her careful English corrections.  
530 Funding from the ANR VMC 2006 - project VULSACO n° ANR-06-VULN-009, the Span-

531 ish Government (CTM2009-11892/IMNOBE project and TM2006-08875/MAR project),  
532 the Netherlands Organisation for Scientific Research (NWO) project 818.01.009, the Uni-  
533 versity of Nottingham and the Juan de la Cierva program are also acknowledged.

## References

- 534 Ashton, A., and A. B. Murray, High-angle wave instability and emergent shoreline  
535 shapes: 1. modeling of sand waves, flying spits, and capes, *J.Geophys.Res.*, *111*,  
536 F04,011,doi:10.1029/2005JF000,422, 2006a.
- 537 Ashton, A., and A. B. Murray, High-angle wave instability and emergent shoreline  
538 shapes: 2. wave climate analysis and comparisons to nature, *J.Geophys.Res.*, *111*,  
539 F04,012,doi:10.1029/2005JF000,423, 2006b.
- 540 Ashton, A., A. B. Murray, and O. Arnault, Formation of coastline features by large-scale  
541 instabilities induced by high-angle waves, *Nature*, *414*, 296–300, 2001.
- 542 Bender, C., and R. Dean, Potential shoreline changes induced by three-dimensional bathy-  
543 metric anomalies with gradual transitions in depth, *Coast. Eng.*, *51*, 1143–1161, 2004.
- 544 Blondeaux, P., Mechanics of coastal forms, *Ann. Rev. Fluid Mech.*, *33*, 339–370, 2001.
- 545 Bruun, P., Migrating sand waves or sand humps, with special reference to investigations  
546 carried out on the Danish North Sea Coast, in *Coastal Eng. 1954*, pp. 269–295, Am.  
547 Soc. of Civ. Eng., 1954.
- 548 Calvete, D., Morphological stability models: Shoreface-connected sand ridges, Ph.D. the-  
549 sis, Appl. Physics Dept., Univ. Politècnica de Catalunya, Barcelona, Spain, 1999.
- 550 Calvete, D., N. Dodd, A. Falqués, and S. M. van Leeuwen, Morphological development  
551 of rip channel systems: Normal and near normal wave incidence, *J. Geophys. Res.*,

552 110(C10006), doi:10.1029/2004JC002803, 2005.

553 Castelle, B., P. Bonneton, H. Dupuis, and N. S en echal, Double bar beach dynamics on  
554 the high-energy meso-macrotidal french aquitanian coast : a review, *Mar. Geol.*, 245,  
555 141–159, 2007.

556 Damgaard, J., N. Dodd, L. Hall, and T. Chesher, Morphodynamic modelling of rip channel  
557 growth, *Coastal Eng.*, 45, 199–221, 2002.

558 Davidson-Arnott, R. G. D., and A. van Heyningen, Migration and sedimentology of long-  
559 shore sandwaves, Long Point, Lake Erie, Canada, *Sedimentology*, 50, 1123–1137, 2003.

560 Dean, R. G., and R. A. Dalrymple, *Coastal Processes*, Cambridge University Press, Cam-  
561 bridge, 2002.

562 Dodd, N., P. Blondeaux, D. Calvete, H. E. de Swart, A. Falqu es, S. J. M. H. Hulscher,  
563 G. R ozy nski, and G. Vittori, The use of stability methods in understanding the mor-  
564 phodynamical behavior of coastal systems, *J. Coastal Res.*, 19(4), 849–865, 2003.

565 Falqu es, A., Wave driven alongshore sediment transport and stability of the Dutch coast-  
566 line, *Coastal Eng.*, 53, 243–254, 2006.

567 Falqu es, A., and D. Calvete, Large scale dynamics of sandy coastlines. Diffusivity and  
568 instability, *J. Geophys. Res.*, 110(C03007), doi:10.1029/2004JC002587, 2005.

569 Falqu es, A., G. Coco, and D. A. Huntley, A mechanism for the generation of wave-driven  
570 rhythmic patterns in the surf zone, *J. Geophys. Res.*, 105(C10), 24,071–24,088, 2000.

571 Falqu es, A., N. Dodd, R. Garnier, F. Ribas, L. MacHardy, P. Larroud, D. Calvete, and  
572 F. Sancho, Rhythmic surf zone bars and morphodynamic self-organization, *Coastal Eng.*,  
573 55, 622–641, doi:10.1016/j.coastaleng.2007.11.012, 2008.

574 Garnier, R., D. Calvete, A. Falqués, and M. Caballeria, Generation and nonlinear evolu-  
575 tion of shore-oblique/transverse sand bars, *J. Fluid Mech.*, 567, 327–360, 2006.

576 Garnier, R., D. Calvete, A. Falqués, and N. Dodd, Modelling the formation and the  
577 long-term behavior of rip channel systems from the deformation of a longshore bar, *J.*  
578 *Geophys. Res.*, 113(C07053), doi:10.1029/2007JC004632, 2008.

579 Garnier, R., N. Dodd, A. Falqués, and D. Calvete, Mechanisms controlling crescentic bar  
580 amplitude, *J. Geophys. Res.*, 115, doi:10.1029/2009JF001407, 2010.

581 Haller, M. C., R. A. Dalrymple, and I. A. Svendsen, Experimental study of  
582 nearshore dynamics on a barred beach with rip channels, *J. Geophys. Res.*, 107(C6),  
583 10.1029/2001JC000,955, 2002.

584 Horikawa, K., *Nearshore Dynamics and Coastal Processes*, University of Tokio Press,  
585 Tokio, Japan, 1988.

586 Inman, D. L., M. H. S. Elwany, A. A. Khafagy, and A. Golik, Nile delta profiles and  
587 migrating sand blankets, in *Coastal Eng. 1992*, pp. 3273–3284, Am. Soc. of Civ. Eng.,  
588 1992.

589 Komar, P. D., *Beach Processes and Sedimentation*, second ed., Prentice Hall, Englewood  
590 Cliffs, N.J., 1998.

591 Lafon, V., D. D. M. Apoluceno, H. Dupuis, D. Michel, H. Howa, and J. M. Froidefond,  
592 Morphodynamics of nearshore rhythmic sandbars in a mixed-energy environment (SW  
593 France): I. Mapping beach changes using visible satellite imagery, *Estuarine, Coastal*  
594 *and Shelf Science*, 61, 289–299, 2004.

595 List, J. H., and A. D. Ashton, A circulation modeling approach for evaluating the condi-  
596 tions for shoreline instabilities, in *Coastal Sediments 2007*, pp. 327–340, ASCE, 2007.

597 List, J. H., D. M. Hanes, and P. Ruggiero, Predicting longshore gradients in alongshore  
598 transport: comparing the cerc formula to delft3d, in *Coastal Eng. 2006*, pp. 3370–3380,  
599 World Scientific, 2006.

600 List, J. H., L. Benedet, D. M. Hanes, and P. Ruggiero, Understanding differences between  
601 delft3d and emperical predictions of alongshore sediment transport gradients, in *Coastal*  
602 *Eng. 2008*, pp. 1864–1875, World Scientific, 2008.

603 MacMahan, J. H., E. B. Thornton, and A. J. H. M. Reniers, Rip current review, *Coastal*  
604 *Eng.*, *53*, 191–208, 2006.

605 Medellín, G., R. Medina, A. Falqués, and M. González, Coastline sand waves on a low  
606 energy beach at 'El Puntal' spit, Spain, *Mar. Geol.*, *250*, 143–156, 2008.

607 Medellín, G., A. Falqués, R. Medina, and M. González, Sand waves on a low-energy beach  
608 at el 'puntal' spit, Spain: Linear Stability Analysis, *J. Geophys. Res.*, *114*(C03022),  
609 doi:10.1029/2007JC004426, 2009.

610 Orzech, M., A. Reniers, E. Thornton, and J. MacMahan, Megacusps on  
611 rip channel bathymetry: Observations and modeling, *Coastal Eng.*, p.  
612 doi:10.1016/j.coastaleng.2011.05.001, 2011.

613 Ozasa, H., and A. H. Brampton, Mathematical modelling of beaches backed by seawalls,  
614 *Coastal Eng.*, *4*, 47–63, 1980.

615 Ranasinghe, R., G. Symonds, K. Black, and R. Holman, Morphodynamics of intermediate  
616 beaches: A video imaging and numerical modelling study, *Coastal Eng.*, *51*, 629–655,  
617 2004.

618 Ranasinghe, R., I. L. Turner, and G. Symonds, Shoreline response to multi-functional  
619 artificial surfing reefs: A numerical and physical modelling study, *Coastal Eng.*, *53*,

620 589–611, 2006.

621 Reniers, A. J. H. M., J. A. Roelvink, and E. B. Thornton, Morphodynamic model-  
622 ing of an embayed beach under wave group forcing, *J. Geophys. Res.*, *109*(C01030),  
623 doi:10.1029/2002JC001586, 2004.

624 Ribas, F., and A. Kroon, Characteristics and dynamics of surfzone transverse finger bars,  
625 *J. Geophys. Res.*, *112*(F03028), doi:10.1029/2006JF000685, 2007.

626 Ruessink, B. G., and M. C. J. L. Jeuken, Dunefoot dynamics along the dutch coast, *Earth*  
627 *Surface Processes and Landforms*, *27*, 1043–1056, 2002.

628 Sonu, C. J., Collective movement of sediment in littoral environment, in *Coastal Eng.*  
629 *1968*, pp. 373–400, Am. Soc. of Civ. Eng., 1968.

630 Sonu, C. J., Three-dimensional beach changes, *J. Geology*, *81*, 42–64, 1973.

631 Stewart, C. J., and R. G. D. Davidson-Arnott, Morphology, formation and migration of  
632 longshore sandwaves; long point, lake erie, canada, *Mar. Geol.*, *81*, 63–77, 1988.

633 Thevenot, M. M., and N. C. Kraus, Longshore sandwaves at Southampton Beach, New  
634 York: observations and numerical simulation of their movement, *Mar. Geology*, *126*,  
635 249–269, 1995.

636 Tiessen, M. C. H., S. M. V. Leeuwen, D. Calvete, and N. Dodd, A field test of a linear  
637 stability model for crescentic bars, *Coastal Engineering*, *57*, 41–51, 2010.

638 USACE, Shore protection manual, *Tech. Rep. 4th ed., 2 Vol.*, USACE, U.S. Government  
639 Printing Office, Washington, D.C., 1984.

640 van den Berg, N., A. Falqués, and R. Ribas, Long-term evolution of nourished beaches  
641 under high angle wave conditions, *Journal of Marine Systems*, *to appear*, 2011.

642 Verhagen, H. J., Sand waves along the dutch coast, *Coastal Eng.*, *13*, 129–147, 1989.

643 Wright, L. D., and A. D. Short, Morphodynamic variability of surf zones and beaches: A  
644 synthesis, *Mar. Geol.*, 56, 93–118, 1984.

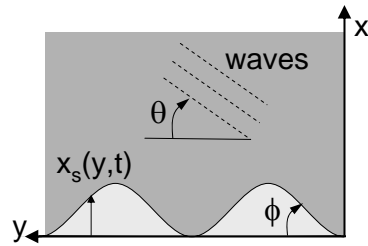


**Figure 1.** Sketch of the geometry and the variables. The angle between the wave fronts and the local shoreline is  $\alpha = \theta - \phi$ .



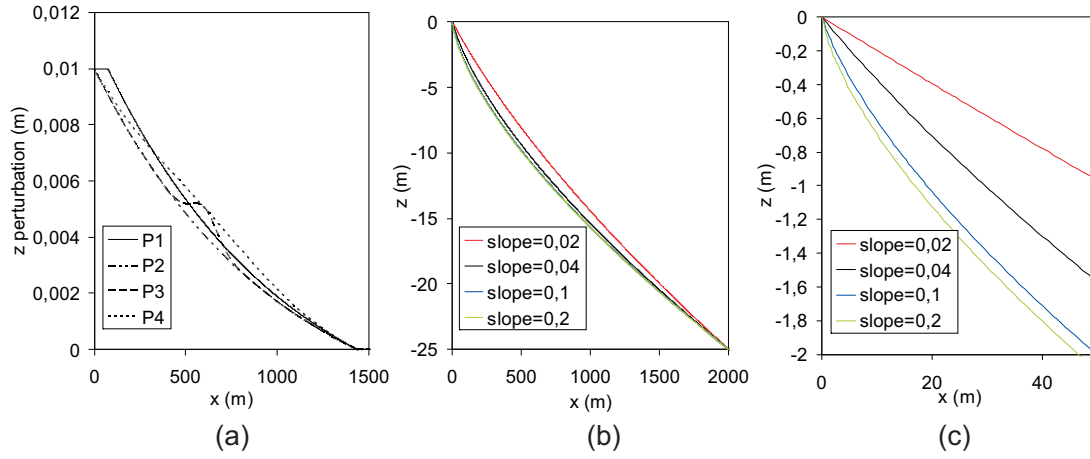


**Figure 2.** Bathymetric perturbations (a) and cross-shore Dean beach profile for a various beach slopes (b,c). P1-perturbation: constant in the surf zone and exponential decrease, P2-perturbation: exponential decrease, P3-perturbation: exponential decrease with a shoal in the shoaling zone, P4-perturbation: exponential decrease with a shoal in the surf and shoaling zones.

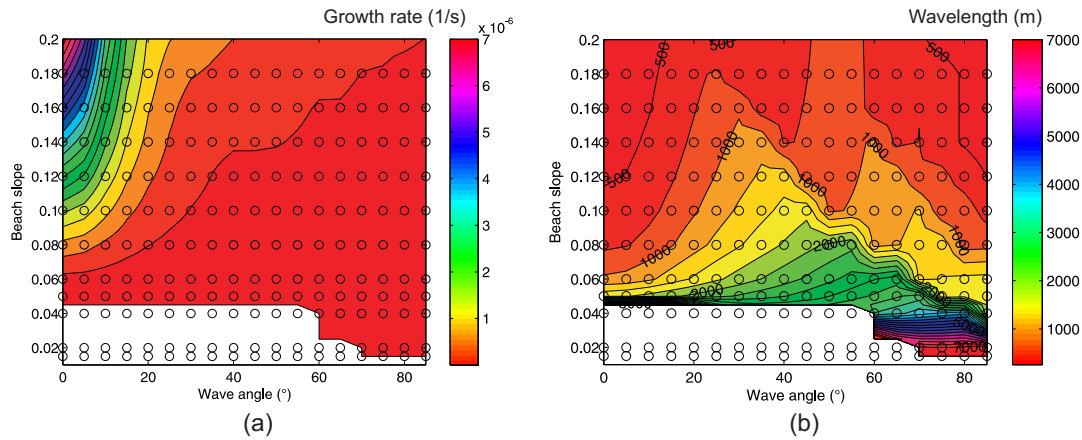


**Figure 3.** LMA (a) growth rate and (b) wavelength as a function of beach slope and angle of incidence. Circles indicate the 1D-morfo computations. In white: no growing perturbation. The model parameters are :  $\mu = 0.15$ ,  $r = 1$ , P1-Perturbation and  $xl=1410$  m for Dean profiles with  $H_{rms} = 1.5$  m and  $T_p = 8$  s at a water depth of 25 m.

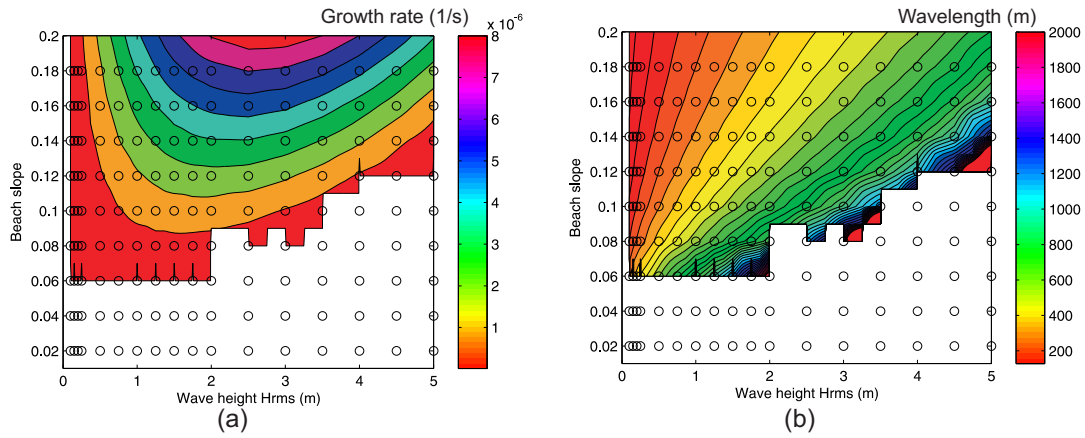


**Figure 4.** LMA (a) growth rate and (b) wavelength as a function of beach slope and wave height, for shore-normal waves. Circles indicate the 1D-morfo computations. In white: no growing perturbation. The model parameters are :  $\mu = 0.15$ ,  $r = 1$ , P1-Perturbation and  $xl=1410$  m for Dean profiles with  $\theta = 0^\circ$  and  $T_p = 8$  s at a water depth of 25 m.

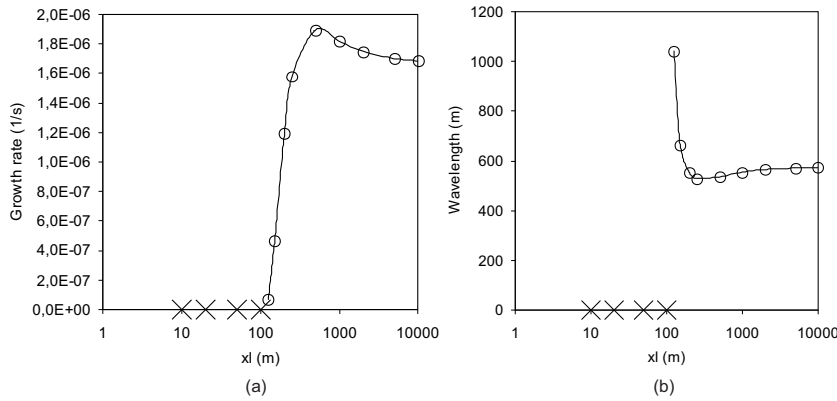


**Figure 5.** LMA mode (a) growth rate and (b) wavelength as a function of the shoreline perturbation length  $xl$  for a Dean profile with a beach slope of 0.1. Crosses on the  $xl$  axis ( $10 \leq xl \leq 100$ ) indicate that there is no LMA mode for the given shoreline perturbation length.

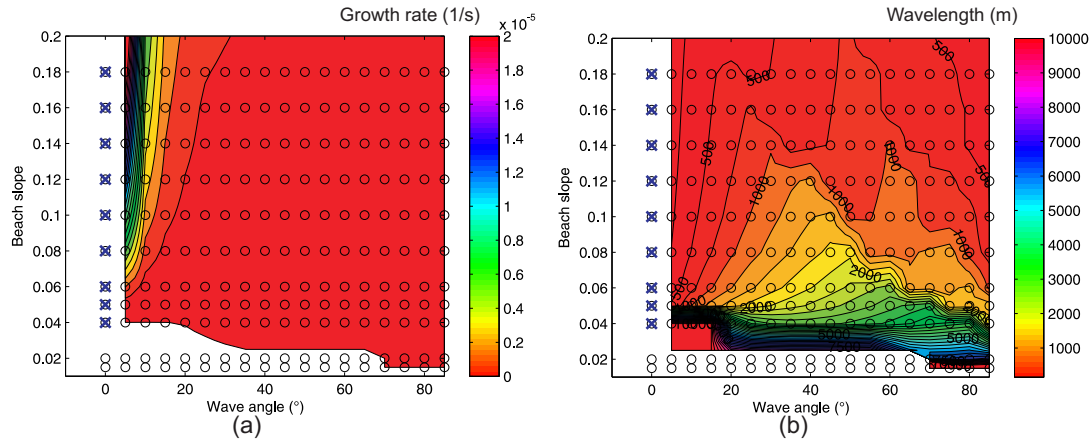


**Figure 6.** LMA (a) growth rate and (b) wavelength as function of beach slope and wave angle, for  $r = 0$ . Circles indicate the 1D-morfo computations. In white: no LMA mode. The symbol x indicates that, even if the growth rate was positive, there was a singularity at  $\theta = 0^\circ$  (growth rate continuously increasing with decreasing wavelength), and therefore no LMA mode (see Figure 7).

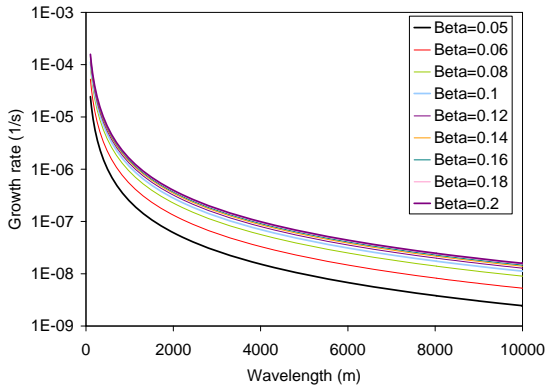


**Figure 7.** LMA growth rate versus wavelength for various beach slopes, using  $r = 0$  and shore-normal waves. The shoreline is stable for a beach slope  $\beta < 0.05$ . The model parameters are :  $\mu = 0.15$ , P1-Perturbation and  $xl=1410$  m for the Dean profile with  $H_{rms} = 1.5$  m and  $T_p = 8$  s at a water depth of 25 m.

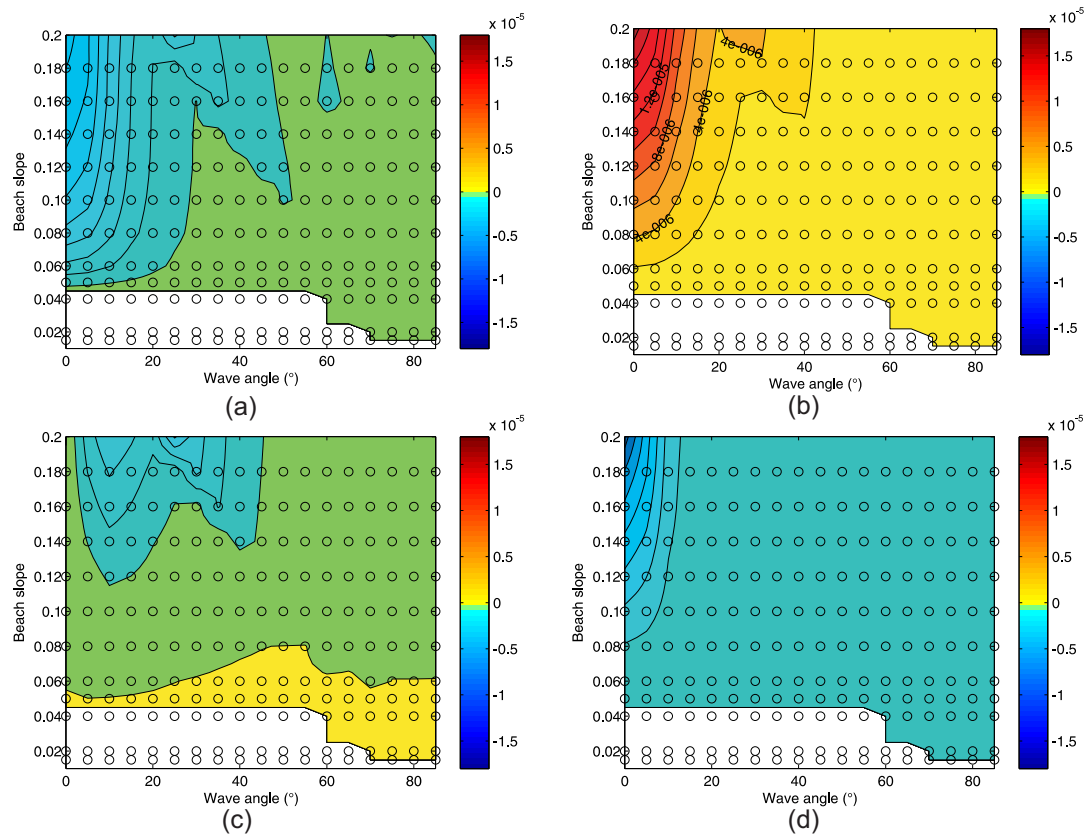


**Figure 8.** Growth rate components for the LMA mode as a function of beach slope and angle of incidence. Model parameters are:  $H_{rms} = 1.5$  m,  $T_p = 8$  s and cross-shore perturbation of type P1 with  $x_l = 1410$  m. (a)  $\sigma_1$ , (b)  $\sigma_2$ , (c)  $\sigma_3$ , (d)  $\sigma_4$ . Circles indicate the 1D-morfo computations. In white: no LMA mode.

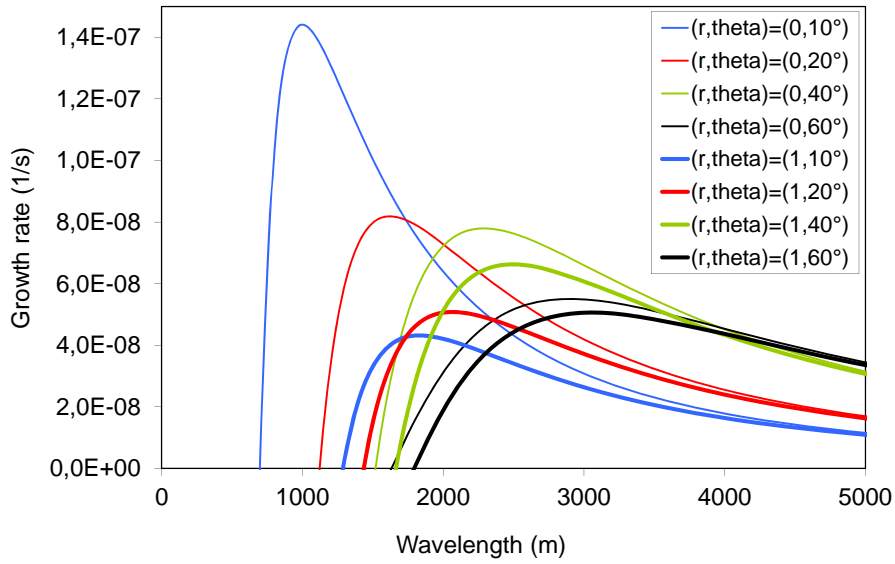


**Figure 9.** Growth rate versus wavelength for several combinations of  $r$  and wave incidence angle  $\theta$ . The beach slope is 0.05.

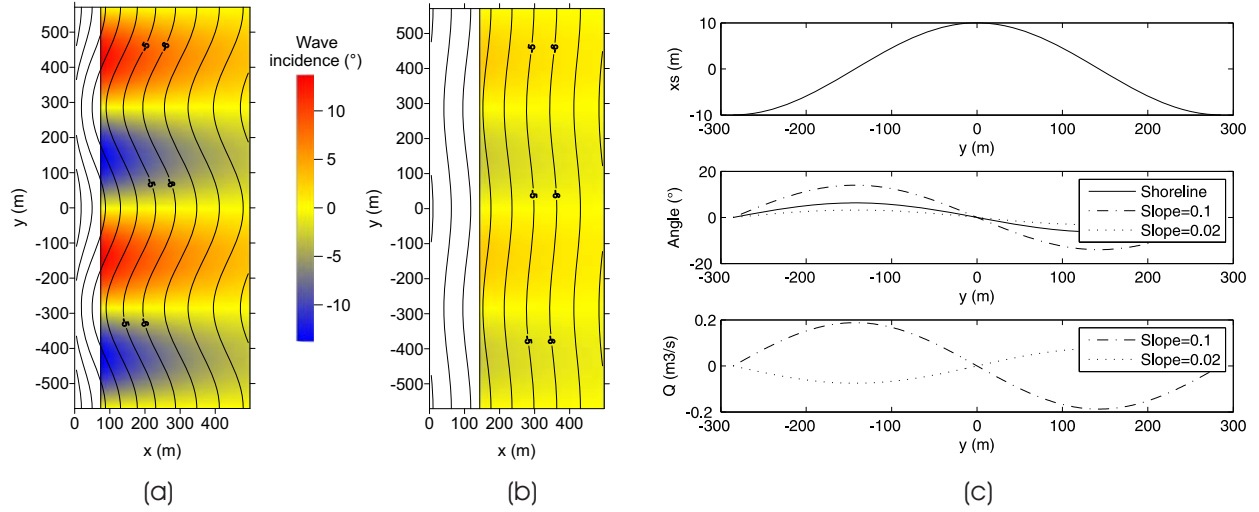


**Figure 10.** Model results for a perturbation wavelength of 571 m (LMA mode for a beach slope of 0.1), shore-normal wave incidence, and a shoreline wave amplitude of  $a = 10$  m. (a) and (b) show the topographic contours and the refracted wave angle for beach slopes of 0.1 (a) and 0.02 (b). (c) shows the longshore profiles of (Top) the shoreline position, (Middle) the shoreline angle (solid line) and refracted wave angles and (Bottom) the sediment fluxes. Dashed-dotted lines, and dotted lines represent a beach slope of 0.1 and 0.02, respectively.

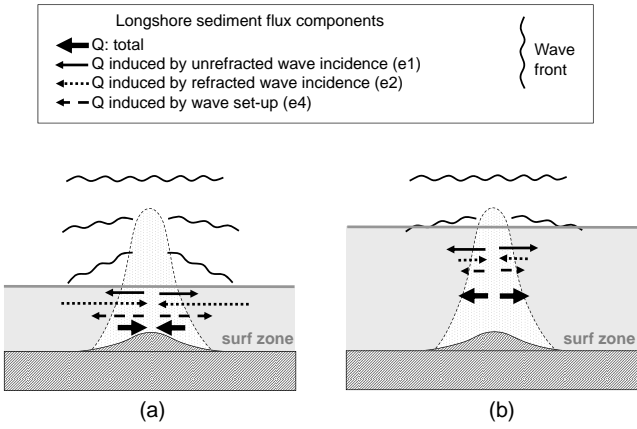


**Figure 11.** Sketch of the physical mechanisms causing LAWI. Sediment transport components induced by a shoal for unstable (a) and stable (b) situations, corresponding to a narrow and wide surf zone, respectively.